Available online at www.sciencedirect.com
SCIENCE DIRECT®
Journal of Nuclear Materials 322 (2003) 180–188
journal of nuclear materials
www.elsevier.com/locate/jnucmat

Ion-beam and electron-beam irradiation of synthetic britholite

S. Utsunomiya [a], S. Yudintsev [b], L.M. Wang [a], R.C. Ewing [a,c,*]

[a] Department of Nuclear Engineering and Radiological Sciences, University of Michigan, Ann Arbor, MI 48109-2104, USA
[b] Institute of Geology of Ore Deposits, Russian Academy of Sciences, Staromonetny 35, 109017 Moscow, Russia
[c] Department of Materials Science & Engineering, University of Michigan, Ann Arbor, MI 48109-2104, USA

Received 12 February 2003; accepted 10 July 2003

Abstract

Britholite, ideally $Ca_{4-x}REE_{6+x}(SiO_4)_6O_2$ (REE = rare earth elements), has the hexagonal structure of apatite, a candidate waste form for actinides. Two synthetic britholites: $Ca_{3.05}Ce_{2.38}Fe_{0.25}Gd_{5.37}Si_{4.88}O_{26}$ (N56) and $Ca_{3.78}La_{0.95}Ce_{1.45}Zr_{0.78}Fe_{0.14}Nd_{2.15}Eu_{0.50}Si_{6.02}O_{26}$ (N88) (*P63*; $Z = 1$) were irradiated with 1.0 MeV Kr^{2+} and 1.5 MeV Xe^{+} over the temperature range of 50–973 K. The process of ion irradiation-induced amorphization, including the effects of the target mass and the ion mass, and the recrystallization of amorphous domains due to ionizing irradiation were investigated. The critical amorphization temperature, T_c was determined to be 910 K for N56 (1.0 MeV Kr^{2+}), 880 K for N88 (1.0 MeV Kr^{2+}) and 1010 K for N88 (1.5 MeV Xe^{+}). The sequence of increasing T_c correlates with the mass of the incident ion; whereas, the ratio of electronic to nuclear stopping power (ENSP) is inversely correlated with T_c. Electron irradiations were conducted on previously amorphized britholite (N56) with an electron flux of 1.07×10^{25} $e^{-}/m^2/s$. The ionizing radiation resulted in recrystallization at the absorbed dose of 6.2×10^{13} Gy. This result suggests that the ionizing radiation can induce recrystallization in silicate apatites, similar to that observed for phosphate apatite.

PACS: 41.75.A; 81.40.E; 61.16.B

1. Introduction

Radiation-induced amorphization of ceramics, including complex-structured minerals, have been examined extensively by in situ ion irradiation experiments using transmission electron microscopy (TEM) [1]. Previous irradiation results for minerals and complex ceramics have recently been compiled in comprehensive reviews [2,3]. One of the motivations for the ion beam irradiation experiments has been to assess the susceptibility of high-level nuclear waste forms to radiation-induced amorphization caused by alpha-decay events [4,5].

Britholite (*P63*; $Z = 1$) is a silicate with the apatite structure [6]. The general formula is $Ca_{4-x}REE_{6+x}(SiO_4)_6O_2$ (REE = rare earth elements). The (SiO_4) tetrahedral monomers are isolated, and there are no bridging oxygens (Fig. 1). Phosphate apatite has a similar structure (*P63/m*; $Z = 1$); the general chemical formula of both the silicate and phosphate is $Ca_{4-x}REE_{6+x}(SiO_4)_{6-y}(PO_4)_yO_2$. In the natural fission reactors located in Gabon, apatite formed due to hydrothermal alteration at temperatures up to 723 K, and the apatite incorporated actinide elements, such as Pu and U (up to 970 ppm) [7]. Thus, apatite has received increased attention as a nuclear waste form for actinides [8] and as a back-fill material in nuclear waste repositories. Apatite has also been reported as a secondary alteration product in corrosion experiments of nuclear waste form glasses; apatite occurred in the outer-most layer of the alteration products of a nuclear waste glass at 473 K [9], and hydroxyapatite also formed as a result of the corrosion of borosilicate nuclear waste glasses at 363 and 473 K as the

* Corresponding author. Address: Department of Nuclear Engineering and Radiological Sciences, University of Michigan, 1906 Cooley Bldg., 2355 Bonisteel Blvd., Ann Arbor, MI 48109-2104, USA. Tel.: +1-734 647 9656/8529; fax: +1-734 647 8531.
E-mail address: rodewing@umich.edu (R.C. Ewing).

0022-3115/$ - see front matter © 2003 Elsevier B.V. All rights reserved.
doi:10.1016/S0022-3115(03)00327-1

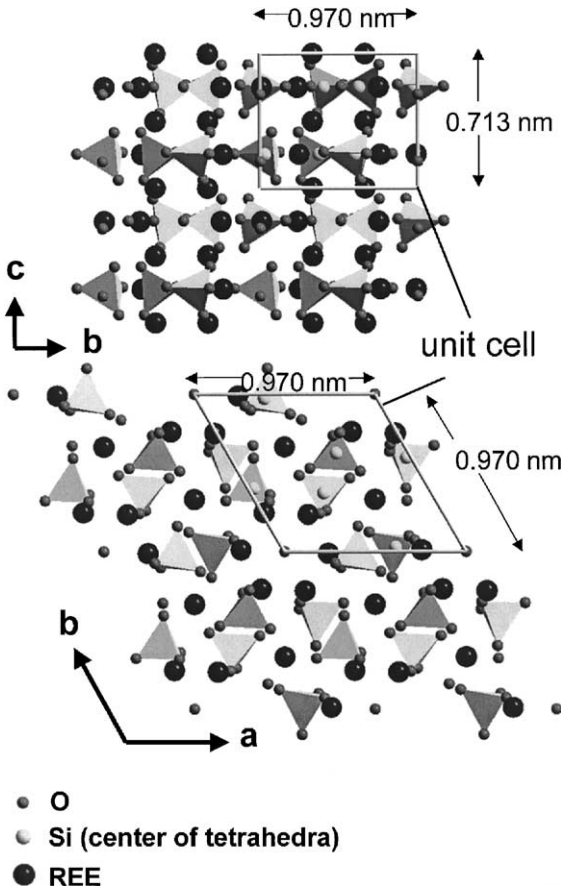

Fig. 1. Schematic illustration of the hexagonal britholite structure along **a*** and **c***. Silicon atoms are located at the centers of the tetrahedra.

pH increased [10]. Thus, the apatite structure-type has been proposed as a potential crystalline ceramic for high-level nuclear waste, particularly for actinide-bearing waste streams [2,8,11,12]. Radiation effects in $Ca_2REE_8(SiO_4)_6O_2$ have been studied in detail by Cm-doping [13–16] and ion beam-irradiation [17–21] experiments. The increase in dissolution rate between crystalline and amorphous britholite, which was initially doped with Cm, was approximately an order of magnitude; the Si release rate from the amorphous britholite was about 13 times greater than that from crystalline britholite, and the actinide release rate was also about 16 times greater than that of crystalline britholite [14]. Damage accumulation for apatite structure-types has been recently compared with other oxides; zircon, perovskite, zirconolite and pyrochlore/fluorite structure-types, and the amorphization dose of the apatite structure was the second lowest among the oxides at ~300 K [22].

Most of the previous studies [13–21] have been completed using britholite with simple compositions. In the present study, two synthetic britholites with very different but complex compositions were synthesized as target materials. Ion irradiation experiments were completed with two different ions; 1.5 MeV Xe^+ or 1.0 MeV Kr^{2+}, in order to evaluate the effect of the target mass and the incident ions. The ion-beam amorphized targets were subsequently irradiated by electrons to examine the effects of ionizing radiation on britholites of complex compositions.

2. Experimental method

The samples were produced by inductive melting of an oxide mixture in a cold crucible. Experiments were performed at a laboratory-scale unit operated at 1.76 MHz with 60 KW power. A cold crucible manufactured from stainless steel pipes was placed within a copper inductor coupled with a high frequency generator.

The chemical compositions of the britholites were determined by electron microprobe analysis, EMPA (Cameca, CAMEBAX). The samples were analyzed by a focused beam spot (~5 μm) with 20 nA and 20 keV. The Cameca PAP correction routine (modified ZAF) was used for data reduction. Interferences from some overlapping peaks for rare earth elements were removed before data reduction.

Back-scattered electron (BE) imaging and semi-quantitative analyses were completed by field emission scanning electron microscopy (FE-SEM, Philips XL30). TEM specimens were prepared by mechanical polishing to a thickness of a few tens of microns, followed by ion milling using 4.0 keV Ar^+. Before ion-irradiation, all TEM specimens were observed by SEM again to make sure of the exact position of britholite in the irradiated section.

The specimens were irradiated with in situ TEM observation using 1.0 MeV Kr^{2+} in the intermediate-voltage electron microscope (IVEM) and 1.5 MeV Xe^+ in the high-voltage electron microscopy (HVEM) at the IVEM/HVEM-Tandem Facility of Argonne National Laboratory [23]. Ion flux was varied between 3.8 and 6.3×10^{15} ions/m^2/s. The specimen temperature during irradiation was from 50 to 1073 K. Selected area electron diffraction (SAED) patterns were used to monitor the amorphization process during intervals of increasing dose. Subsequent observations were completed by high resolution TEM (HRTEM, JEOL 2010F). The critical amorphization fluence, F_c, in ions/m^2 was converted to critical dose, D_c, in the unit of displacement per atom (dpa) [24,25] and to the kinetic energy transferred to each target atom through nuclear collision (E_n) using SRIM2000 [26]. The equations for the conversion are

$$\text{dpa} = \frac{F_c \times [\text{displacements by single ion per nm}] \times 10^3}{[\text{atomic density}]}. \quad (1)$$

With high-energy ions used in this study, most of ions penetrate through the thin TEM specimen, and the displacement damage level through the sample thickness is relatively uniform:

$$E_n = \frac{E'_n \times D_c \times 10^8}{[\text{atomic density}]}, \quad (2)$$

$$E'_n = E_R - I_R + P_I, \quad (3)$$

where E_R, I_R and P_I are the ion energy loss to recoil atoms, the recoil ionization energy loss and the incident ion energy loss to phonons, respectively. In the calculation for britholite used in the present experiments, the displacement threshold energy, E_d, was assumed to be 15 eV for Si, 28 eV for O and 25 eV for the other cations [26].

After the amorphization was completed by the ion irradiation, the effect of ionizing irradiation was investigated by electron irradiation at 200 keV. The electron flux was 1.07×10^{25} $e^-/m^2/s$, and the beam current was 7.6 nA.

3. Results

The chemical compositions of the synthetic britholites used in the present experiments are given in Table 1. The britholites have complex compositions, including REE, Ca, Zr, and Fe. BSE images in Fig. 2 show that euhedral crystals of britholite up to ~50 μm in size. The surrounding matrix consists of garnet ($A_3B_2(XO_4)_3$) and wollastonite ($CaSiO_3$).

Both ion irradiations by Kr^{2+} and Xe^+ resulted in amorphization of the britholite at room temperature, as evidenced in the SAEDs shown in Fig. 3 (N88 by 1.5 MeV Xe^+). The SAED patterns show a gradual decrease in the intensity of the diffraction maxima and the development of a diffuse halo of scattered X-rays characteristic of an amorphous material. HRTEM micrographs show the radiation-induced transition in N88 (1.5 MeV Xe^+) at room temperature. Amorphous domains (approximately a few nanometers in size) appeared sparsely within the britholite crystalline matrix at the early stage (0.050 dpa in Fig. 4(b)), and the amorphous fraction gradually increased with dose (0.074 dpa in Fig. 4(c)). Eventually, the britholite was fully amorphous at 0.15 dpa (Fig. 4(d)). Ion irradiation of N56 also revealed the same radiation-induced transition from the crystalline to amorphous state at room temperature.

The critical amorphization doses, D_c (dpa), at various temperatures are given in Table 2. E_n values are also tabulated. The D_c as a function of temperature for the three irradiation conditions are plotted in Fig. 5. The resulting curve shows the typical exponential increase in D_c as proposed by Weber et al. [27]. The critical amorphization dose (dpa) was almost constant below 800 K, but it increased rapidly at higher temperatures, >800 K. The D_c–T curves of N56 and N88 irradiated by 1.0 MeV Kr^{2+} intersected. The critical amorphization temperature, T_c, above which the material does not become amorphous state, was estimated to be 910 K for N56

Table 1
Chemical composition (in wt%) of britholites analyzed by EMPA

	SiO_2	CaO	La_2O_3	CeO_2	ZrO_2	Fe_2O_3[a]	Nd_2O_3	Eu_2O_3	Gd_2O_3
N56	20.6	12.0	–	28.7	–	1.39	–	–	38.7
N88	23.4	13.7	9.98	16.7	6.25	0.73	23.5	5.71	–

[a] All Fe given as Fe_2O_3.

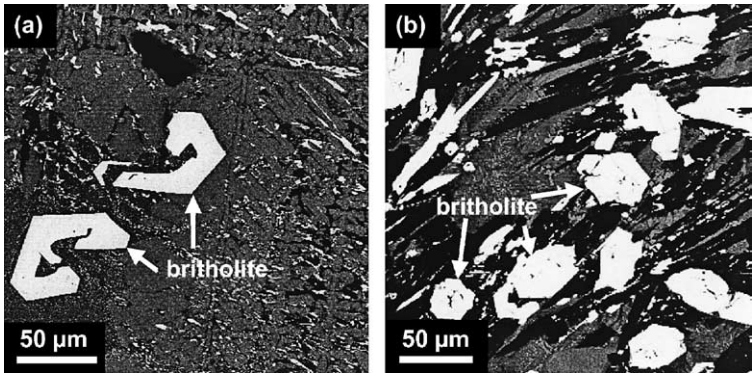

Fig. 2. Back-scattered electron images of the target materials: (a) N56 and (b) N88. Gray areas are garnet, dark areas are wollastonite.

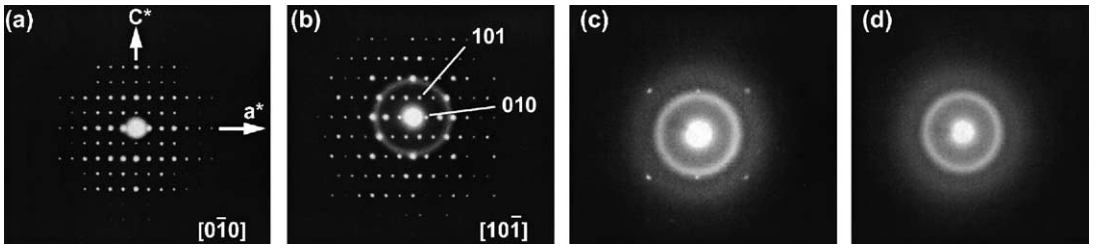

Fig. 3. The selected area electron diffraction (SAED) patterns showing the transition from crystalline to amorphous state for N88 under 1.5 MeV Xe^{+} irradiation at room temperature: (a) 0 dpa, (b) 0.050 dpa, (c) 0.074 dpa, and (d) 0.15 dpa.

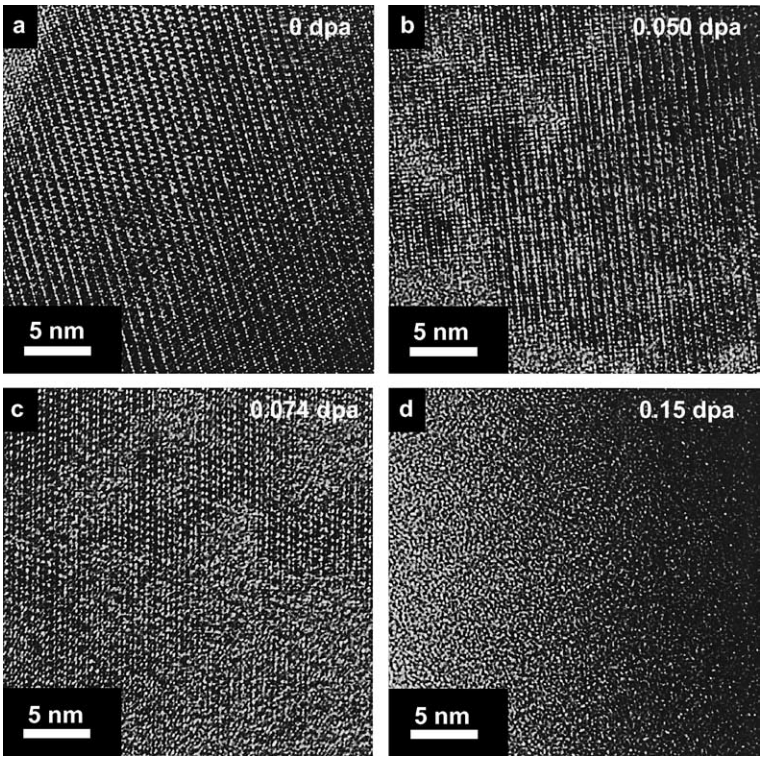

Fig. 4. The high-resolution TEM images showing the crystalline-to-amorphous transition in N88 under 1.5 MeV Xe^{+} irradiation at room temperature: (a) 0 dpa, (b) 0.050 dpa, (c) 0.074 dpa, and (d) 0.15 dpa.

Table 2
Summary of the critical amorphization dose in displacement per atom (dpa) and the energy loss through nuclear collision (E_n) (eV/atom) for each irradiation

Temperature (K)	N56 (1.0 MeV Kr^{2+})		N88 (1.0 MeV Kr^{2+})		N88 (1.5 MeV Xe^{+})	
	dpa	E_n	dpa	E_n	dpa	E_n
50	0.27	17	–	–	0.13	8.0
298	0.40	26	0.31	20	0.15	8.9
523	0.50	32	–	–	–	–
773	0.85	54	0.35	22	0.33	20
823	–	–	0.64	41	–	–
853	–	–	1.3	81	–	–
873	3.0	187	5.6	353	0.42	25
973	–	–	–	–	2.2	131

(1.0 MeV Kr^{2+}), 880 K for N88 (1.0 MeV Kr^{2+}) and 1010 K for N88 (1.5 MeV Xe^{+}). The temperatures were close to the recovery temperature (823 K) of amorphous, Cm-doped $Ca_2Nd_8(SiO_4)_6O_2$ [13,15].

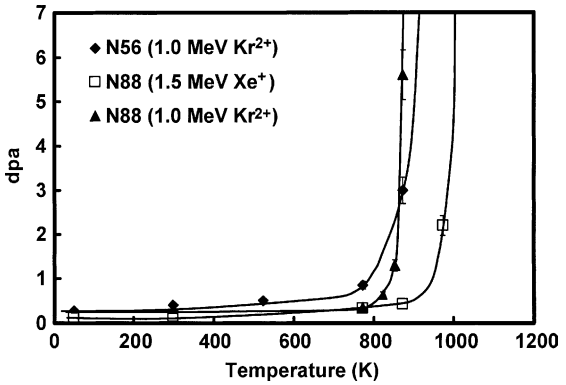

Fig. 5. The temperature dependences of D_c for the three irradiation conditions.

The amorphous britholite (N56) was subsequently irradiated by 200 keV electrons at room temperature. After only 7 min of irradiation (fluence = 4.5×10^{27} e^{-}/m^2), crystals nucleated (Fig. 6(c)). Eventually (fluence = 8.6×10^{27} e^{-}/m^2), the nanocrystals grew to be 20–30 nm in size (Fig. 6(d)). The nanocrystals were identified based on the SAED patterns as having the britholite-structure.

4. Discussion

4.1. Effects of target mass and ion mass on D_c and T_c

Evaluation of the mass effect of target and incident ion is of great importance because these effects can result in an increase or decrease of D_c and even in a shift of T_c. In addition, the susceptibility of target materials to

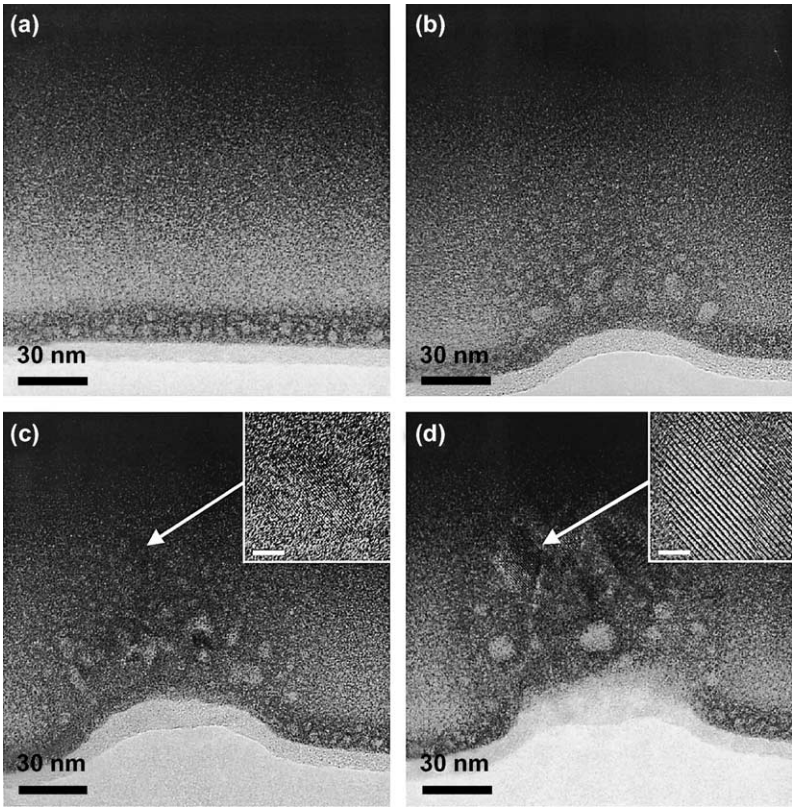

Fig. 6. The sequence of TEM images with increasing dose under 200 keV electron irradiation for N56 at room temperature. The electron beam current was 7.62 nA. The N56 was initially amorphous due to a previous 1.0 MeV Kr^{2+} irradiation (a). After 3 min, 1.93×10^{27} e^{-}/m^2 (b); 7 min, 4.49×10^{27} e^{-}/m^2 (c) and 13 min, 8.35×10^{27} e^{-}/m^2 (d). The inset of (c) showing a nucleation of crystals appeared after 7 min of irradiation. Eventually, the britholite recrystallized as shown by the high-resolution image (inset) (d). The insets of (c) and (d) are the filtered high-resolution images for which the background has been subtracted. The scale bars in the insets are 5 nm.

amorphization appears to change slightly as a function of composition for britholite. Once the trend of mass effects is clarified, the results from ion-irradiation experiments in many simple ceramics might be used to predict radiation effects in the more complex compositions that will be typical of actual nuclear waste forms.

The simple parameter for the evaluation of the mass effects is the maximum transferable kinetic energy to the target based on a classical two particle scattering model. Although it is difficult to use the parameter to evaluate the energy transfer in a multi-compound target, target mass and the ion mass make the same contribution to the efficiency of kinetic energy transfer, which implies that the effect of target mass on the damage process should be the same as the effect changes in the ion mass.

The other approach used to predict mass effects is based on a model of cascade formation in which epitaxial recrystallization occurs at the boundary of the cascade, shrinking the volume of damage domains [28]. For irradiations with heavy ions that form larger cascades, the relatively larger amorphous domains are less easily recrystallized than smaller cascade volumes because of the smaller surface to volume ratio. Thus, D_c decreases and T_c increases as the target mass or the ion mass increase [28].

Table 3 summarizes the values of parameters that cause T_c (K) to vary; the initial kinetic energy, E_0 (MeV); displacement efficiency (displacement/ion/nm); the electronic and the nuclear stopping powers calculated by SRIM2000, dE/dx_e and dE/dx_n (eV/nm), respectively; and the ratio of electronic to nuclear stopping power (ENSP). The effect of target mass on the susceptibility to amorphization within a fixed structure type has been shown for phosphates [29], perovskite [30], zirconolite [31], pyrochlore [32] and garnet with complex chemical composition [33]. All of the previous results have shown that the T_c shifts to higher temperature as the mass of the target increases. For the same target material (N88), the heavier incident ion led to a higher T_c. The parameter, ENSP, can also be used to evaluate the variation in T_c. Based on experiments by Zinkle [34,35] that correlate the rate of dislocation loop formation and ENSP [34,35], the larger the ENSP, the higher the mobility of defects, thus enhancing annealing. This annealing effect causes the shift to higher D_c and a lower T_c [29]. In fact, ionizing radiation has been previously shown to promote recrystallization or annealing of the amorphous domains [19,20,36,37]. In the present work, the ENSP also varied inversely with T_c. The effects of ion mass and the energy of the incident ions have also been discussed by Wang et al. [28], in which a heavier incident ion corresponds to a larger stopping power and thus a larger subcascade size [38,39]. In Wang et al.'s study [28], T_c increased with increasing subcascade radius as calculated by TRIM [26] using three different ions [28].

Table 3
Summary of parameters used to discuss the variation in T_c; the initial kinetic energy, E_0 (MeV); the critical amorphization temperature, T_c (K); the displacement efficiency (displacement/ion/nm), E_{dis}, at the thickness of 100 nm; the electronic and the nuclear stopping powers calculated by SRIM2000, dE/dx_e and dE/dx_n (eV/nm) which are the average value through the sample thickness, respectively; the ratio of electronic to nuclear stopping power (ENSP)

	N56	N88	
E_0	1.0 MeV	1.0 MeV	1.5 MeV
T_c	910	880	1010
E_{dis}	7.0	6.5	11
dE/dx_e	930	930	1280
dE/dx_n	720	700	1230
ENSP	1.29	1.33	1.04

The effects of ion mass have also been discussed in a previous study [40]. Weber and others completed ion-irradiations of zircon using a low energy heavy ion, 0.6 MeV Bi, and concluded that the relatively lighter ions of He to Xe do not provide an accurate simulation of the D_c and T_c for alpha-decay events, because the D_c for Bi in their study were about twice as large as the D_cs of lighter ions through the entire temperature range [40]. However, the effect of changes in ion mass on T_c in their data is complicated by experimental limitations. The difficulty is the result of the limited penetration range of the low energy heavy ions. There are two issues related to measuring the D_c using low energy heavy ions during an in situ TEM study. As discussed by Wang [41], the damage profile of an incident ion must not have an abrupt change within the thickness of the specimen that is normally monitored by SAED (~200 nm). For the conditions of the previous study [40], the SRIM2000 calculation ($E_d = 79$ for Zr, 23 for Si and 47 for O [2]; the density was 4.670; the incident ions were 0.6 MeV Bi, 0.8 MeV Xe and 0.8 MeV Kr) showed that the ion distribution of Bi has a maximum at a thickness of 100 nm, and all of the ions have stopped within the 200 nm thickness. In contrast, the ion distribution of Kr and Xe showed the maxima at 300 and 200 nm, respectively, and more than half of the ions passed completely through the specimen. In the former case, the measured amorphization dose for the Bi irradiation is more difficult to determine because most of the ions do not pass through the examined sample thickness, and a substantial fraction of undamaged material remains within the examined thickness of the sample. This means that a significant portion of the examined thickness has a much lower damage dose than calculated. Another issue is the procedure used to convert from ion fluence to dpa in the heavy-ion irradiations. When the fluence, F_c, is converted to dpa, the collision events calculated by SRIM2000 must be used as shown in Eq. (1). The average number of the collision events through the sample

thickness is generally used for the calculation. However, the number of collision events calculated using SRIM2000 for the Bi irradiation have a non-linear distribution with values varying from 0.0 to 30 (displacement/ion/nm); whereas, Kr and Xe results showed the average number of collision events to be 9.0 and of 17 (displacement/ion/nm), respectively, without large deviations from the average value. Thus, one can use the average values of Kr and Xe as being representative of the number of collision events throughout the entire thickness of the examined sample.

4.2. Ionizing irradiation-induced crystallization

Electron irradiation by a focused beam (7.6 nA) after the complete amorphization of N56 resulted in the polycrystalline recrystallization of the amorphous britholite at room temperature. The electron irradiation generally causes a temperature rise and radiolysis due to ionization. The temperature rise due to focused beam can be estimated using a model of electron radiation [42,43]. The model by Fisher has been generally used [36,37]. According to the modified model by Jenic et al. [44,45] solving the Gausian distribution of electron in the beam, the temperature rise, ΔT, is can be calculated by

$$\Delta T = \frac{I}{4\pi\lambda e_0}\left(\frac{\mathrm{d}E}{\mathrm{d}x}\right)\left[1 + 2\ln\frac{b}{r_0}\right], \tag{4}$$

where I is the beam current, λ is the thermal conductivity of the sample, e_0 is the electron charge, r_0 is the effective beam radius, b is the radius of the heat sink, and $-\mathrm{d}E/\mathrm{d}x$ is the stopping power for electrons, which is given by the Bethe equation [46]. For the irradiation at the edge of the sample, the equation is

$$\Delta T_{\mathrm{hole}} = \frac{I}{\pi\lambda e_0}\left(\frac{\mathrm{d}E}{\mathrm{d}x}\right)\ln\frac{b}{r_0}. \tag{5}$$

Based on Bethe's equation [46], the stopping-power of electrons in MeV/m is

$$-\frac{\mathrm{d}E}{\mathrm{d}x} = \frac{4\pi k_0^2 e_0^4 n}{mc^2\beta^2}\left[\ln\frac{mc^2\tau\sqrt{\tau+2}}{\sqrt{2}I_{\mathrm{ex}}} + F(\beta)\right] \times \frac{1}{1.60\times10^{-13}}, \tag{6}$$

where

$$F(\beta) = \frac{1-\beta^2}{2}\left[1 + \frac{\tau^2}{8} - (2\tau+1)\ln 2\right], \tag{7}$$

$\tau = E_{\mathrm{kin}}/mc^2$, in which E_{kin} is the kinetic energy, thus τ is the multiple of the electron rest energy mc^2, $k_0 = 1/4\pi\varepsilon_0$, in which ε_0 is the permittivity constant, e is the magnitude of the electron charge, n is the number of electrons per unit volume in the medium, m is the electron rest mass, c is the speed of light in vacuum, β is the ratio of the speed of the particle to the light (V/c), I_{ex} is the mean excitation energy of the medium, which is expressed by the following empirical formulas:

$$I_{\mathrm{ex}} \cong \begin{cases} 19.0\ \mathrm{eV} & Z = 1\ \text{(hydrogen)}, \\ 11.2 + 11.7Z\ \mathrm{eV} & 2 \leqslant Z \leqslant 13, \\ 52.8 + 8.71Z\ \mathrm{eV} & Z > 13, \end{cases} \tag{8}$$

where Z is the atomic number of the target. For complex compositions, I_{ex} can be calculated by summing the contributions from the individual constituent elements:

$$n\ln I_{\mathrm{ex}} = \sum_i N_i Z_i \ln I_i, \tag{9}$$

N_i is atomic density (atoms/m^3) for an element with atomic number Z_i and its mean excitation energy I_i.

The electronic stopping power was calculated to be 404 and 441 MeV/m for N56 and N88, respectively. Because the exact thermal conductivity of the amorphous material used here is unknown, the λ was assumed to be the same as the value for SiO_2 (amorphous); 1.4 w/m K [47]. The temperature rise caused by the current (7.6 nA) was calculated to be ~6 K in the present specimen. Obviously the temperatures were not high enough to reach the T_c of these materials. Thus, the ionizing effect by electron irradiation caused the recrystallization. The absorbed electronic dose when the recrystallization occurred was calculated to be 6.2×10^{13} Gy using the electronic stopping power deduced above. The recrystallization dose is high as compared with the total absorbed dose due to β-decay, ~10^{10} Gy, in commercial high-level waste form [48]. In addition, the dose rate can be more important for recrystallization processes than the total electronic dose as previously reported [37]. Thus, a low dose rate for absorbed ionizing radiation in an actual repository may not result in recrystallization of the amorphous domains.

Recrystallization to a polycrystalline texture was previously reported in simple silicates with the apatite structure, $Ca_2La_8(SiO_4)_6O_2$ [21]. In their study, the target was simultaneously irradiated by both ions and electrons at near the T_c. The polycrystals were produced by the ion irradiation with 1.5 MeV Kr^+ at 673 K, which is near T_c. On the other hand, the polycrystals in the present study were ascribed mainly to the effects of ionizing radiation, because the experiments were carried out at room temperature. In [20], $Ca_2La_8(SiO_4)_6O_2$ was irradiated by 1.5 MeV Xe^+ with and without a 300 keV electron irradiation. The amorphization dose with electron irradiation was more than twice as high as the dose without electron irradiation [20]. These previous studies

suggested that an electron irradiation cause the annealing effects in silicates with the apatite structure. The recrystallization of amorphous domains by ionizing radiation has also been observed in other ceramics: phosphate [36], zircon [36], fluoapatite [37], hydroxyapatite [37].

5. Conclusions

Ion irradiation experiments with 1.0 MeV Kr^{2+} and 1.5 MeV Xe^{+} were completed for two synthetic, chemically complex britholites at temperatures between 50 and 973 K. Both the ion mass and target mass had the same effect on the critical amorphization temperature, T_c; that is, T_c increased as either the target mass or the ion mass increased. ENSP was used to explain the T_c variation, which had an inverse correlation. In addition, electron-irradiation induced recrystallization occurred at room temperature in the amorphous domains created by the ion irradiations. The calculated rise in temperature ($\sim$6 K) was not enough to reach T_c. Therefore, the electron beam irradiation results suggest that the apatite structure is highly susceptible to recrystallization of amorphous domains by ionizing radiation.

Acknowledgements

The authors thank the staff of the HVEM/IVEM-Tandem Facility at Argonne National Laboratory for assistance during the ion irradiation experiments. S.U. thanks the staff of the Electron Microbeam Analysis Laboratory at University of Michigan and Chris Palenik for help with the EMPA. This work was supported by US DOE, Office of Basic Energy Sciences under grant DE-FGO2-97ER45656.

References

[1] L.M. Wang, R.C. Ewing, MRS. Bull. 17 (1992) 38.
[2] W.J. Weber, R.C. Ewing, C.R.A. Catlow, T. Diaz de la Rubia, L.W. Hobbs, C. Kinoshita, Hj. Matzke, A.T. Motta, M. Nastasi, E.K.H. Salje, E.R. Vance, S.J. Zinkle, J. Mater. Res. 13 (1998) 1434.
[3] R.C. Ewing, A. Meldrum, L.M. Wang, S.X. Wang, Rev. Miner. Geochem. 39 (2000) 319.
[4] R.C. Ewing, W.J. Weber, F.W. Clinard Jr., Prog. Nucl. Ener. 29 (1995) 63.
[5] R.C. Ewing, Proc. Nat. Acad. Sci. USA 96 (1999) 3432.
[6] N. Kalsbeek, S. Larsen, J.G. Ronsbo, Zeit. Kristallogr. 191 (1990) 249.
[7] R. Bros, J. Carpena, V. Sere, A. Beltritti, Radiochim. Acta 74 (1996) 277.
[8] R.C. Ewing, L.M. Wang, Rev. Miner. Gechem. 39 (2002) 673.
[9] W.L. Gong, R.C. Ewing, L.M. Wang, E. Vernaz, J.K. Bates, W.L. Ebert, Mater. Res. Soc. Symp. Proc. 412 (1996) 197.
[10] W.L. Ebert, J.K. Bates, W.L. Bourcier, Waste Manag. 11 (1991) 205.
[11] W.J. Weber, H.J. Matzke, Radiat. Eff. 98 (1986) 93.
[12] J. Carpena, F. Audubert, D. Bernache, L. Boyer, B. Donazzon, J.L. Lacout, N. Senamaud, Mater. Res. Soc. Symp. Proc. 506 (1998) 543.
[13] W.J. Weber, J. Am. Ceram. Soc. 65 (1982) 544.
[14] W.J. Weber, Radiat. Eff. 77 (1983) 295.
[15] W.J. Weber, Nucl. Instrum. and Meth. B 65 (1992) 88.
[16] W.J. Weber, J. Am. Ceram. Soc. 76 (1993) 1729.
[17] W.J. Weber, R.K. Eby, R.C. Ewing, J. Mater. Res. 6 (1991) 1334.
[18] W.J. Weber, L.M. Wang, Nucl. Instrum. and Meth. B 91 (1994) 63.
[19] W.J. Weber, R.C. Ewing, A. Meldrum, J. Nucl. Mater. 250 (1997) 147.
[20] R. Devanathan, K.E. Sickafus, W.J. Weber, M. Nastasi, J. Nucl. Mater. 253 (1998) 113.
[21] L.M. Wang, W.J. Weber, Philos. Mag. A 79 (1999) 237.
[22] W.J. Weber, R.C. Ewing, Mater. Res. Soc. Symp. Proc. 713 (2002) 443.
[23] C.W. Allen, L.L. Funk, E.A. Ryan, S.T. Ockers, Nucl. Instrum. and Meth. B 40&41 (1989) 553.
[24] R.K. Eby, R.C. Ewing, R.C. Birtcher, J. Mater. Res. 7 (1992) 3080.
[25] S.X. Wang, L.M. Wang, R.C. Ewing, R.H. Doremus, J. Non-Cryst. Sollids 238 (1998) 198.
[26] J.F. Ziegler, J.P. Birsak, U. Littmark, The Stopping and Range of Ions in Solids, Pergamon Press, New York, 1985.
[27] W.J. Weber, R.C. Ewing, L.M. Wang, J. Mater. Res. 9 (1994) 688.
[28] S.X. Wang, L.M. Wang, R.C. Ewing, Phys. Rev. B 63 (2000) 024105-1.
[29] A. Meldrum, L.A. Boatner, R.C. Ewing, Phys. Rev. B 56 (1997) 13805.
[30] A. Meldrum, L.A. Boatner, R.C. Ewing, Nucl. Instrum. and Meth. B 141 (1998) 347.
[31] S.X. Wang, G.R. Lumpkin, L.M. Wang, R.C. Ewing, Nucl. Instrum. and Meth. B 166&167 (2000) 293.
[32] S.X. Wang, L.M. Wang, R.C. Ewing, K.V. Govindan Kutty, Nucl. Instrum. and Meth. B 169 (2000) 135.
[33] S. Utsunomiya, L.M. Wang, S. Yudintsev, R.C. Ewing, J. Nucl. Mater. 303 (2002) 177.
[34] S.J. Zinkle, Nucl. Instrum. and Meth. B 91 (1994) 234.
[35] S.J. Zinkle, J. Nucl. Mater. 219 (1995) 113.
[36] A. Meldrum, L.A. Boatner, R.C. Ewing, J. Mater. Res. 12 (1997) 1816.
[37] A. Meldrum, L.M. Wang, R.C. Ewing, Am. Miner. 82 (1997) 858.
[38] H. Abe, H. Naramoto, A. Iwase, C. Kinoshita, Nucl. Instrum. and Meth. B 127&128 (1997) 681.
[39] S.X. Wang, L.M. Wang, R.C. Ewing, G.S. Was, G.R. Lumpkin, Nucl. Instrum. and Meth. B 148 (1999) 704.
[40] W.J. Weber, R. Devanathan, A. Meldrum, L.A. Boatner, R.C. Ewing, L.M. Wang, Mater. Res. Soc. Symp. Proc. 540 (1999) 367.
[41] L.M. Wang, Nucl. Instrum. and Meth. B 141 (1998) 312.
[42] S.B. Fisher, Radiat. Eff. 5 (1970) 239.

[43] M. Liu, L.Y. Xu, X.Z. Lin, Scanning 16 (1994) 1.
[44] I. Jencic, M.W. Bench, I.M. Robertson, M.A. Kirk, J. App. Phys. 78 (1995) 974.
[45] I. Jencic, I.M. Robertson, J. Mater. Res. 11 (1996) 2152.
[46] J.E. Turner, Atoms, Radiation, and Radiation Protection, 2nd Ed., John Wiley, New York, 1995, p. 555.
[47] T. Knight, Thermal properties of materials. Home page: <http://www.ai.mit.edu/people/tk/tks/tcon.html>.
[48] W.J. Weber, R.C. Ewing, C.A. Angell, G.W. Arnold, A.N. Cormack, J.M. Delaye, D.L. Griscom, L.W. Hobbs, A. Navrotsky, D.L. Price, A.M. Stoneham, M.C. Weiberg, J. Mater. Res. 12 (1997) 1946.